Brune, S., Ladage, S., Babeyko, A. Y., Müller, C., Kopp, H., Sobolev, S. V. (2009): Submarine landslides at the eastern Sunda margin: observations and tsunami impact assessment. - Natural Hazards, 54, 2, 547-562

DOI: 10.1007/s11069-009-9487-8

Submarine landslides at the eastern Sunda margin: observations and tsunami impact assessment

Sascha Brune [1*], Stefan Ladage [2], Andrey Y. Babeyko [1], Christian Müller [2], Heidrun Kopp [3], Stephan V. Sobolev [1]

[1] *Helmholtz Centre Potsdam GFZ German Research Centre for Geosciences, Potsdam, Telegrafenberg, 14473 Potsdam, Germany*
[2] *Federal Institute for Geosciences and Natural Resources (BGR), Stilleweg 2, 30655 Hannover, Germany*
[3] *Leibniz Institute of Marine Sciences at the Christian-Albrechts University of Kiel (IFM-GEOMAR), Wischhofstr. 1-3, 24148 Kiel, Germany*
[*] *Corresponding author. e-mail: brune@gfz-potsdam.de*

Abstract
Our analysis of new bathymetric data reveals six submarine landslides at the eastern Sunda margin between central Java and Sumba Island, Indonesia. Their volumes range between 1 km³ in the Java fore-arc basin up to 20 km³ at the trench off Sumba and Sumbawa. We estimate the potential hazard of each event by modeling the corresponding tsunami and its run-up on nearby coasts. Four slides are situated remarkably close to the epicenter of the 1977 tsunamigenic Sumba M_w=8.3 earthquake. However, comparison of documented tsunami run-up heights and arrival times with our modeling results neither allows us to confirm nor to decline the hypothesis that the earthquake triggered these submarine landslides.

Keywords**:** Submarine landslide; Tsunami; Numerical modeling; Indonesia; Padang; Hazard assessment

1 Introduction
Tsunamis pose a major threat to population and structures in many coastal areas around the world. Although most tsunamis are generated by submarine earthquakes, underwater slope failures can be responsible for local tsunamis as well. Landslide-generated tsunamis comprise at least 8 % of all documented historical events worldwide (ITDB catalogue 2007). That makes the investigation of submarine landslides a necessary step for future tsunami hazard assessment. One of the best studied historical events took place in Papua New Guinea, 1998, where a 4 km³ submarine slump was triggered by a comparatively small earthquake (Tappin et al. 1999; Sweet and Silver 2003). The generated tsunami inundated nearby coasts, leading to maximal run-up heights of 15 m (Lynett et al. 2003). Whether a submarine mass movement generates significant wave amplitudes, depends on its volume, water depth, shape and its velocity profile. Associated inundation heights depend mainly on the tsunami propagation distance and local bathymetry. If the tsunami hits land after a few kilometers, even small landslides (0.0024 km³ slide at Fatu Hiva, French Polynesia, 1999 (Hébert et al. 2002)) can cause significant damages to coastal communities. Very large events like the 200 km³ 1929 Grand Banks slide (Fine et al. 2005) or the 2400 km³ pre-historic Storegga slide (Bondevik et al. 2005) were capable of generating large run-up even hundreds of kilometers away.

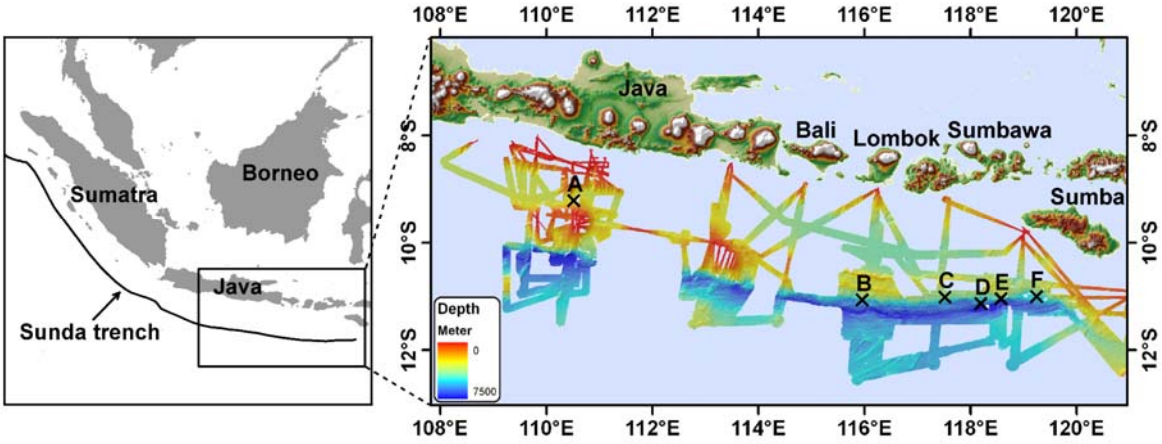

Figure 1 *Overview map showing bathymetric coverage and locations of slides A to F.*

Indonesia is especially endangered by tsunamis, due to its proximity to the Sunda subduction zone stretching over 5000 km from the Andaman Islands and Sumatra to Java, and the Lesser Sunda Islands. The subduction of the Indo-Australian plate beneath the Sunda shelf creates tectonic stresses which upon sudden release cause earthquakes of major magnitudes that potentially generate large tsunamis (Hamzah et al. 2000). The M_w=9.3 Sumatra-Andaman earthquake in December, 2004 ruptured over 1000 km (Krüger and Ohrnberger 2005) and induced a catastrophic ocean-wide tsunami. Run-up heights reached more than 30 m in Aceh, Indonesia (Borrero et al. 2006) and nearly 20 m in Thailand (Tsuji et al. 2006). Off Java and the Lesser Sunda Islands, devastating tsunamis were induced by the M_w=8.3 Sumba earthquake of 1977, the eastern Java earthquake (M_w=7.8) of 1994 and the M_w=7.7 Pangandaran earthquake in 2006 (ITDB catalogue 2007). Maximum run-up values of respectively 8 m (Kato and Tsuji 1995), 14 m (Tsuji et al. 1995a) and 20 m (Lavigne et al. 2007; Fritz et al. 2007) have been identified.

By triggering submarine mass failures, however, even moderate earthquakes can induce dangerous tsunamis. Large local run-up during the 1979 tsunami at Lomblen Island and in 1992 at the northern coast of Flores Island has been explained by underwater mass failures (Tsuji et al. 1995b; Rynn 2002). Whether the above mentioned 20 m run-up during the 2006 Central Java tsunami was caused by a landslide, is currently discussed (Matsumoto et al. 2007). Submarine debris avalanches have been identified west of Sumatra (Tappin et al. 2007), at the toe of the accretionary prism. The overall slide volume of the largest event is with 1 km³ (Moran and Tappin 2006) comparably small which excludes it as a significant tsunami source (Tappin et al. 2007).

Our present study is based on new bathymetric data collected onboard the RV “Sonne” during the MERAMEX (2004) and SINDBAD (2006) surveys. The multibeam bathymetry data has a resolution of 2° (corresponding to 200 m at ocean depths of 6000 m). The cruises have been conducted by two German institutions: IFM-GEOMAR, Kiel, and the Federal Institute for Geosciences and Natural Resources (BGR), Hannover. Our

study area comprises the eastern Sunda margin off Indonesia, between central Java and Sumba (Figure 1). Detailed analysis of the bathymetry data revealed evidences of six landslide events. We start with a short geological background of the studied area and proceed with detailed slide descriptions and numerical models of the tsunamis generated during these events.

2 Geological setting

The over 5000 km long Sunda margin extends from the Andaman Sea in the north to Sumba Island in the east. It is characterized by the subduction of oceanic lithosphere of the Indo-Australian plate beneath the Indonesian Archipelago. East of Sumba Island a transition to the Banda Arc and the collision with continental Australian crust takes place. Subduction initiated in the late to middle Tertiary (Hall 1997) and has formed a mature convergent margin with a well developed accretionary prism, an outer fore-arc high and fore-arc basins (Schlueter et al. 2002; Kopp and Kukowski 2003).

The eastern Sunda Arc sector from East Java to just west of Sumba Island resembles a unique segment of this subduction zone. Here, the oldest oceanic crust along the entire Sunda Arc of Late Jurassic age (155-145 Ma; Heine et al. 2004; Müller et al. 2008) subducts at a rate of up to 70 mm per year in nearly trench normal direction (Simons et al. 2007). With water depths reaching more than 7000 m, this is also the deepest segment of the Java trench. Off eastern Java the sediment thickness on the incoming plate and in the trench is less than 1 km (Kopp et al. 2003). Further east the oceanic crust and trench are largely devoid of sediments, except for a thin hemipelagic sediment cover. The accretionary wedge in the eastern segment is between 70-100 km wide and forms a discontinuous outer fore-arc high with maximal water depths exceeding 2000 m. Internally, the accretionary wedge is built up of a series of landward dipping imbricate thrust sheets of accreted and deformed rocks (Lueschen et al., submitted; van der Werff 1995).

Off eastern Java the Roo Rise, elevated about 1500 m above surrounding sea floor, is recently subducting and causing frontal erosion of the accretionary wedge (Kopp et al. 2006). Further east the Java trench morphology is rugged and controlled by normal faulting of the oceanic crust with horst and graben structures along the outer trench wall. The faults are more than 60 km long and have a throw of 500 m. They strike slightly oblique to the trench and can be imaged deep beneath the slope toe. Subduction of these faults and horst and grabens contributes to local oversteepening of the slope toe with slumping (van der Werff 1995; Müller et al. 2008; Lueschen et al., submitted). The distribution and focal mechanisms of shallow seismicity along the Java trench clearly shows recent activity of these faults (Eva et al. 1988; Spence 1986).

3 Slide descriptions

We analyzed the bathymetric data searching for head scarp walls and associated landslide deposits. Six major subrecent landslides have been identified within the studied area. In the following, they will be designated alphabetically from A to F (Figure 1). Slide A is located within the Java fore-arc basin, 120 km off coast. Slide B was found at the

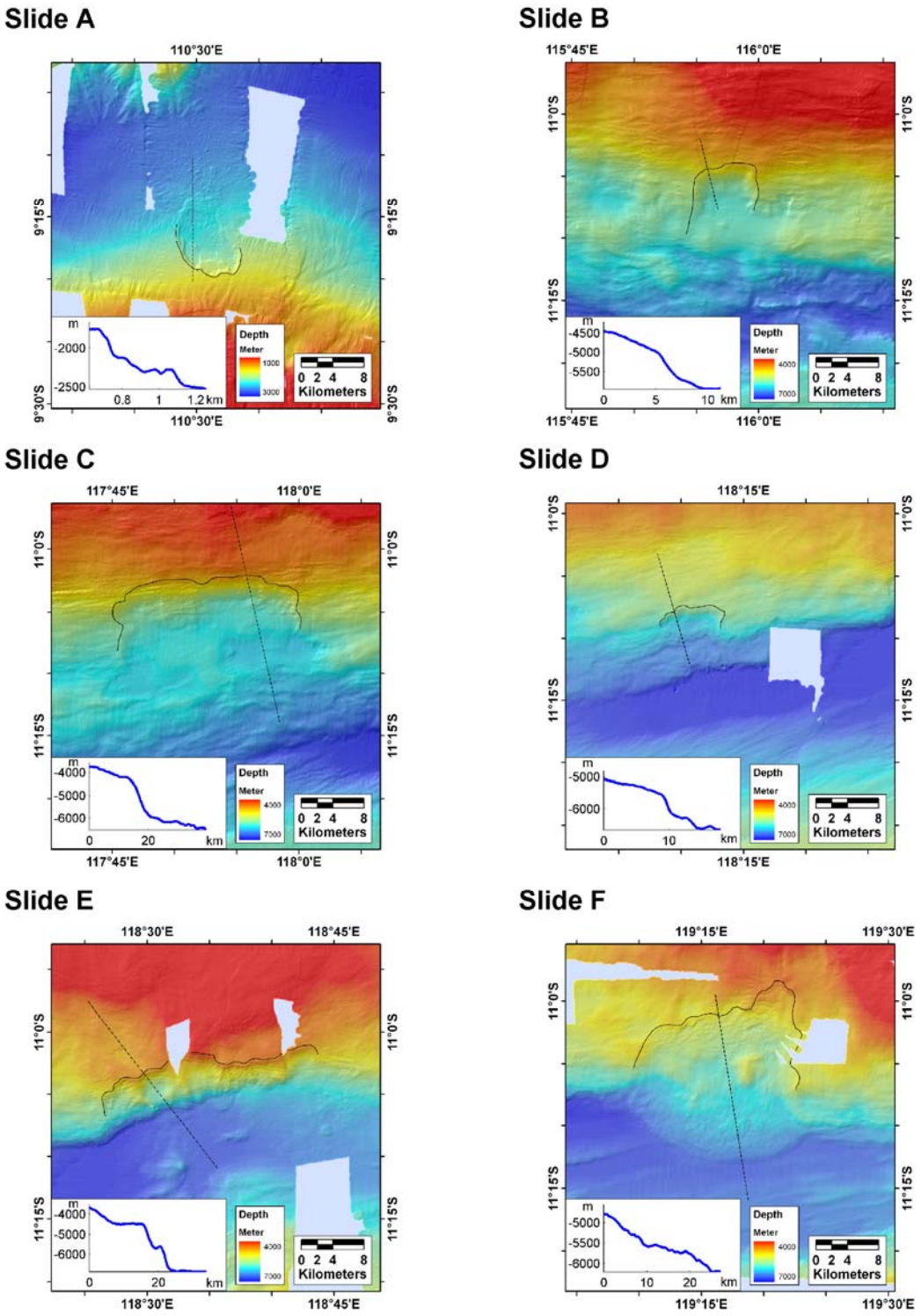

Figure 2 *Bathymetry maps, interpretations of the escarpments (solid lines) and locations of cross sections (dashed lines). Corresponding profiles are shown in white inlets. Note the different depth scale for slide A. Slide locations are mapped in Figure 1.*

accretionary wedge 240 km off Lombok and slides C to F near the trench, at a distance of 130 to 200 km to Sumba Island.

The deposition lobes of slides A and F are clearly visible (Figure 2). Their shape and proximity to the failure area suggest rotational slumping as probable failure mechanism. Typical features of translational slides like slide tracks or sidewalls are not visible which supports the hypothesis of rotational failure. In the cases B, C, D, and E, the depositional area is barely observable. We analyzed backscatter data, 3.5 kHz sub-bottom - and multichannel-reflection seismic profiles. Landslide head scarps were identified, however associated landslide sediment deposits were not detectable. The position of the slides and their geometrical parameters (for nomenclature see Figure 3) are deduced from the bathymetric maps and listed in Table 1. In the following, we concentrate on determining the necessary input parameters for our tsunami generation routine (see section 4.1 and Supplement). Slide dimensions perpendicular and parallel to the slope, denoted as width and length, respectively, range between 4 and 25 km. The travel distance which corresponds to the center of mass translation, is obvious only for the cases A and F, as they exhibit typical deposit lobes. Travel distances estimated for the other four slides comprise rather high uncertainties. We evaluate the slide heights by comparing the slope profile inside the slide zone and besides it. This yields values between 100 m for slide D and up to 300 m for slide E and F. Slide volumes of slides A to F (3 km³, 4 km³, 15 km³, 1 km³, 15 km³, and 20 km³, respectively) are estimated based on slide height, length and width. We therefore assumed a smooth slide shape with parabolic profiles in direction of both length and width.

It is very difficult to date underwater mass movements based on bathymetric images only. As submarine diffusion rates are notably smaller than on land, landscapes evolve much slower. So, even a “fresh” looking slide can be thousands of years old (McAdoo and

	Slide A	Slide B	Slide C	Slide D	Slide E	Slide F
Longitude	110°31’E	115°57’E	117°52’E	118°12’E	118°34’E	119°15’E
Latitude	9°18’S	11°6’S	11°4’S	11°9’S	11°4’S	11°3’S
Width (km)	7	7	23	7	25	18
Length (km)	8	7	8	4	5	10
Height (m)	150	200	200	100	300	300
Volume (km³)	3	4	15	1	15	20
Depth (m)	2000	5300	5300	6000	6100	5000
Travel Distance (km)	6	4	12	4	5	10
Mean local slope angle (°)	4	15	10	8	15	5

Table 1 *Slide parameters. Longitude and latitude designate the estimated initial center of mass location. Width is measured perpendicular, and length parallel to the slope. Volume is inferred by parabolic shape approximation. Travel distance denotes the estimated movement of the slide’s center of mass. Mean local slope angles are inferred from bathymetry cross-sections of slide areas.*

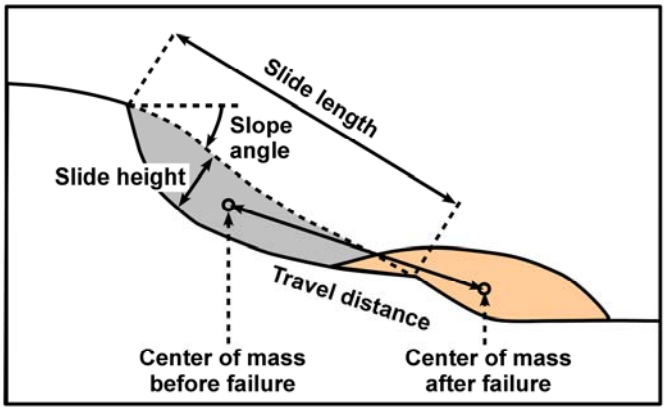

Figure 3 *Sketch of key slide parameters. Slide length denotes lateral dimension in down slope direction. Slope angle is averaged over slide length. Slide height represents maximum thickness of the slide body. Travel distance designates horizontal center of mass dislocation.*

Simpson 2005). Dating techniques involving the steepness of the head wall are only applicable if at least one additional independent failure date is provided by a secondary method (Kukowski et al. 2008). In this region, this has not been done so far. However, in section 5 we investigate the possibility that slides C to F have been triggered by the 1977 Sumba earthquake (M_w=8.3). If confirmed, this would also imply the age of the slumps.

Most submarine slope failures are caused by interplay of several factors like oversteepening of slopes and ground shaking due to an earthquake (Masson et al. 2006). At the position of slide A, basin slopes have been possibly steepened due to the subduction of a seamount located on the oceanic plate (Masson et al. 1990; Kopp et al. 2006). Concerning the other five events at the slope toe in the trench, oversteepening can be attributed to tectonic erosion (Kopp et al. 2006). For slopes close to failure, even a comparatively small earthquake is sufficient to induce a landslide.

4 Modeling of induced tsunamis

4.1 Methods

Our tsunami model consists of three distinct stages: generation, propagation and run-up. We describe tsunami generation using the technique of Watts et al. (2005) and Grilli et al. (2005). It provides a set of semi-empirical equations that are based on physical arguments and wave tank experiments. The initial tsunami wave height η_{2HD}, the wave length λ and the characteristic time of slide motion t_0 (Table 2) are estimated based on landslide geometry parameters length, width, height, depth and travel distance as well as the mean local slope angle (Table 1). This method and the employed formulas are summarized in the Supplementary.

Following Watts et al. (2003), an initial wave distribution can be used to approximate the sea surface deformation provoked by the mass movement. It is argued that during the acceleration phase of a slide, most of the tsunami energy is invested in potential energy.

	Slide A	Slide B	Slide C	Slide D	Slide E	Slide F
Initial wave height η_{2HD} (m)	2.9	1.0	6.4	0.4	8.8	7.0
Characteristic wave length λ (km)	19	23	27	20	15	27
Characteristic time t_0 (s)	130	100	120	80	60	120

Table 2 *Hotstart parameters defining the initial sea surface for the tsunami propagation model. Their calculation follows the technique of Watts et al. (2005).*

The characteristic time t_0 designates the moment after failure when the wave build-up is finished and transformation of potential energy into kinetic energy takes place. The initial sea surface was constructed according to Watts et al. (2005) and Synolakis et al. (2002): Along slide direction, two Gaussian curves of different sign approximate the wave profile. Their heights correspond to η_{2HD} and the widths are defined by λ. To extend this one-dimensional profile to the slide-perpendicular direction, a solitary-like extrapolation proportional to the factor $\mathrm{sech}^2(3 \cdot y/(w+\lambda))$ is used, where w is the slump width and y the corresponding coordinate. The semi-empirical equations are applicable as long as wave breaking can be excluded. To ensure this, the ratio of slide length to initial submergence depth must be smaller than 17 (Watts et al. 2005). The corresponding values of slide A to F (4, 1.3, 1.5, 0.7, 0.8 and 2, respectively) clearly satisfy this condition.

Alternative formulations include a dynamic slide movement that continuously influences the surface wave, like the shallow water approach of Harbitz (1992) or the Boussinesq model of Lynett and Liu (2002). These models allow for a more detailed slide description, however, they are only valid if the ratio of slide length to submergence depth is bigger than 30 for shallow water models or 7 for Boussinesq simulations (Lynett and Liu 2002). In our case, with length to depth ratios between 0.7 and 4, these formulations cannot be used.

The tsunami propagation is modeled with the finite difference, nonlinear shallow water code TUNAMI-N2 (Imamura et al. 1997). The shallow water approximation is fulfilled, as all wave lengths are much larger than the water depth. Tsunami calculations are performed on a 3200×2200 grid using a spatial step size of 10 arc seconds (~309 m) and a time step of 0.5 s. Bathymetry is based on interpolated GEBCO data (IOC, IHO and BODC 2003).

Realistic computation of tsunami inundation and run-up necessitates highly resolved (~50 m) near-shore bathymetry and topography (see e.g., Titov and Synolakis 1997). This resolution is not available; instead we use interpolated GEBCO grid of 1 nautical mile resolution. For the estimation of run-up, an approach similar to Geist and Parsons (2006) is adopted. We extrapolate near-shore wave amplitudes to final run-up heights R employing the formula of Ward and Asphaug (2003): $R = A^{4/5} \cdot d^{1/5}$, where A is the wave

amplitude, measured at water depth *d*. (Geist and Parsons 2006 implied a constant amplification factor of 2). Analogue to Green's law, this formula is based on the conservation of wave energy flux in linear theory, however, it has the advantage of avoiding divergence for small water depths. It can be used for both breaking and non-breaking waves (Ward and Asphaug 2003). The formula can reproduce 'true run-up' only to a certain degree, as the later is heavily dependent on local ground elevation and wave form. Hence, we refer to the results obtained with the above formula as effective 'estimated run-up heights'. In this paper we use virtual gauges at depths of approximately 20 m. In section 8 (Supplementary material), we address the influence of the choice of water depth *d* on the estimated run-up height *R*.

4.2 Results

Figure 4 presents distributions of the maximum tsunami heights for the slides A to F. Although events A, B and D involve significant slide volumes (3 km³, 4 km³, 1 km³, respectively) they do not generate significant tsunamis (estimated run-up heights generally do not exceed 1 m).

The volumes of slides C, E, and F (15 km³, 15 km³, 20 km³) are considerably larger than those mentioned before. Generated tsunamis feature initial wave heights of 6 to 7 m. As the tsunami propagates, it is influenced by the regional bathymetry (Satake 1988). So, the central part of the wave front is diffracted eastward by the underwater onset of the Sumba strait (Figure 4, slides C and E). Similarly, off-shore seafloor elevations focus the wave energy, as can be seen for Sumbawa (Slide C and E) and Sumba (Slide E). Estimated run-up heights for each event are shown in Figure 4 by blue bars. Maximum run-up heights of nearly 6 m are estimated on Sumbawa for slide C and E. A run-up of 7 m is reached in Leterua on Sumba for slide F.

Tsunami arrival times vary between 20 and 30 minutes for all areas exposed to large wave heights (here arrival time corresponds to the first 1 cm sea surface anomaly). Arrival times for slide D are only shown at locations experiencing water elevations of more than 1 cm (Figure 4).

While slide width and in some cases slide length can be estimated from bathymetric data quite accurately, both height and travel distance are subjected to a higher uncertainty. We systematically varied these parameters within the possible range that we estimated from bathymetry data. Projected to near-shore amplitudes, this uncertainty can be responsible for up to 50 % variation.

5 Triggering of landslides by the 1977 Sumba M_w=8.3 earthquake?

The 1977 Sumba earthquake (M_w=8.3; Lynnes and Lay 1988) was the biggest event in our study area during the 20th century (ITDB catalogue 2007), and one of the largest normal fault earthquakes ever recorded. Its epicenter (11° 8' S, 118° 14' E; CMT catalogue) is located about 200 km southwest of Sumba Island. The earthquake generated a tsunami which inundated the coasts of Sumba, Sumbawa, Lombok, and Bali resulting in 440 damaged houses and 161 casualties or missing (Kato and Tsuji 1995). In Figure 5, we mapped the epicenter location, the seven-days aftershock distribution and the assumed

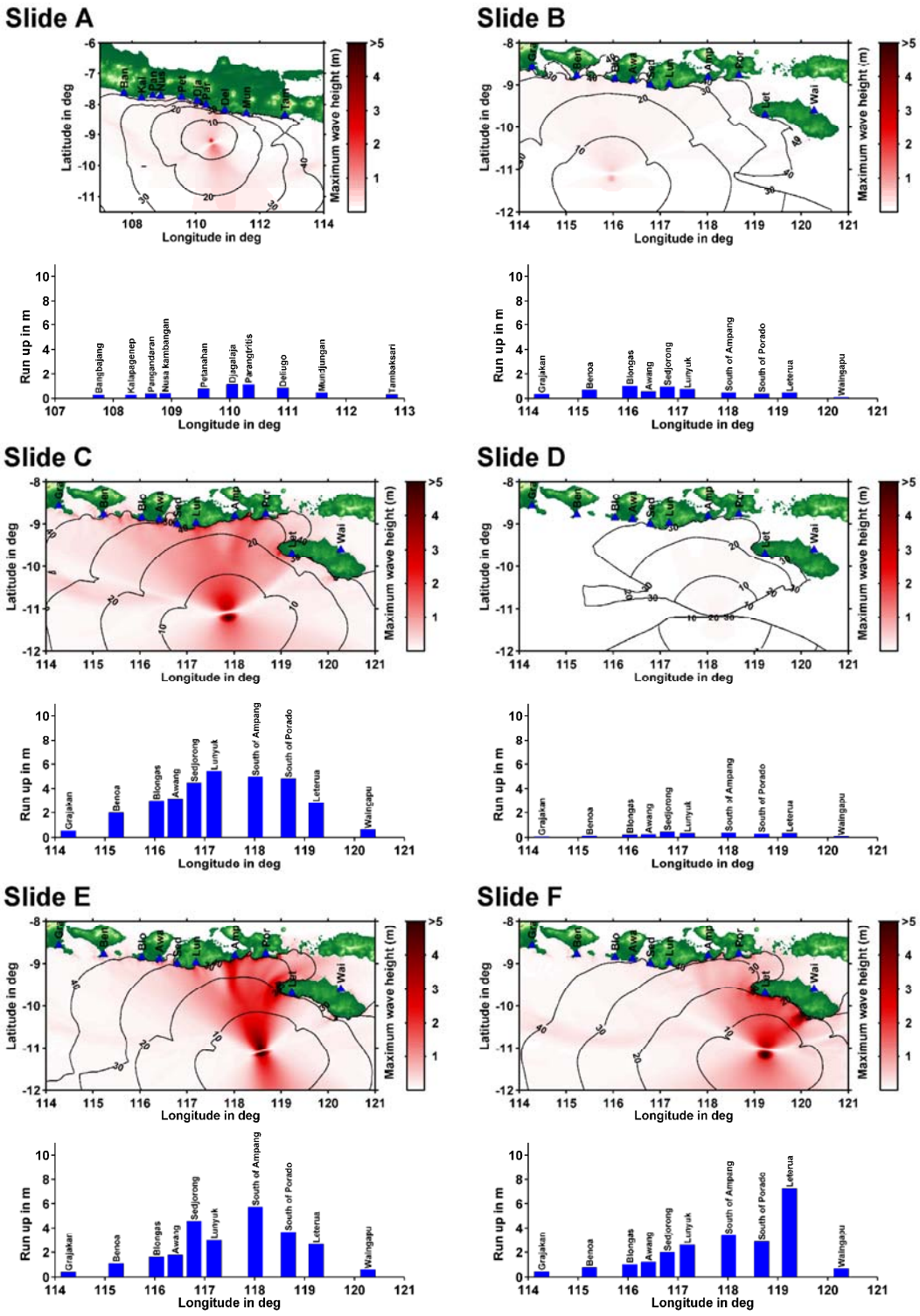

Figure 4 *Maximum wave height distributions after 4 hours, arrival times in minutes as well as corresponding estimated run-up heights along the coast projected onto the longitude (bar plots). Locations of virtual gauge stations are mapped as blue triangles with abbreviated names.*

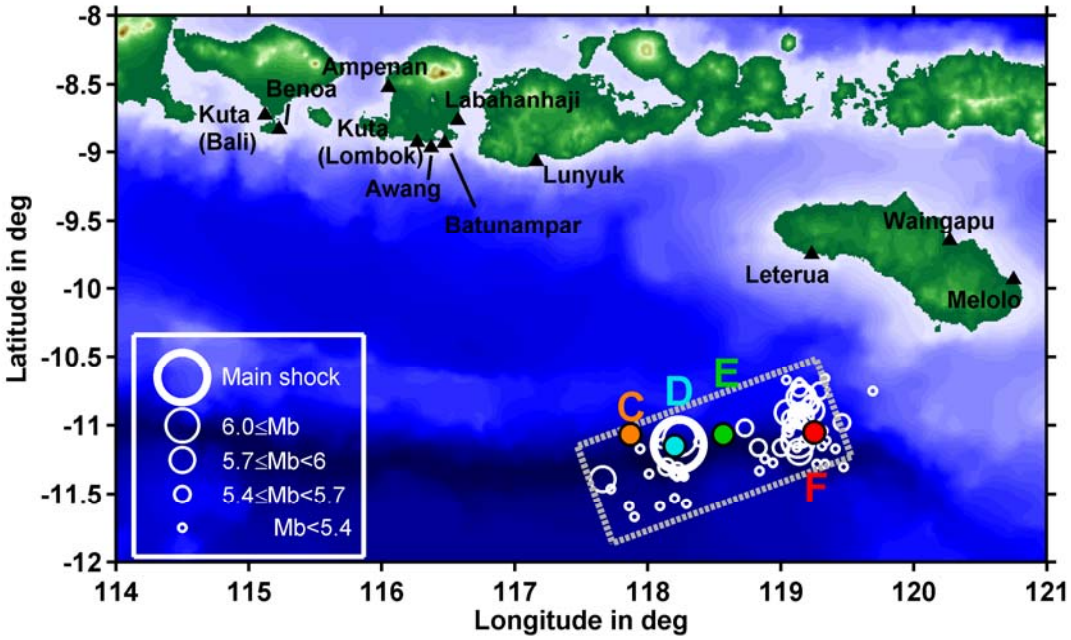

Figure 5 *1977 Sumba earthquake: Main shock location, seven-days aftershock distribution and assumed fault plane (dotted rectangle). Also designated are positions of slides C to F as well as locations of the measured run-up (black triangles).*

fault plane. Interestingly, slides C to F are located directly above the fault plane. The location of slide F coincides with an area of high aftershock intensity. This raises the questions whether one or more of the slides might have been triggered by the earthquake, and whether these slides may have modified the earthquake-generated tsunami. As our knowledge about the slumps is based on remote sensing only, we cannot determine the age of the events and whether they failed during the earthquake. However, an ITIC survey team and Indonesian investigators visited the tsunami affected areas and determined run-up heights and arrival times (ITIC 1977). That gives us the opportunity to compare results of an earthquake tsunami model to surveyed data. Thereby, we can test if possible discrepancies might be explained by an additional landslide source.

5.1 Comparison by run-up

The survey accessed eight locations on Bali and Lombok. Due to difficult accessibility, only two places on Sumbawa and three on Sumba have been visited, whereof two are situated on the far side of the island. Survey locations are mapped in Figure 5. Measured run-up values are given with respect to the sea level at time of measurements (ITIC 1977). For our study, we use run-up data that was corrected for astronomical tides (Kato and Tsuji 1995). These run-up values are shown in Figure 6a. If more than one run-up is given for the same location, minimal and maximal values are marked in deep and light blue, respectively.

Based on the aftershock distribution (Figure 5), we assess the following earthquake parameters: centroid location 118.5°E, 11.2°S, rupture extension 195 km, fault plane width 65 km and strike 70°. The fault plane is slightly wider as if one had used the

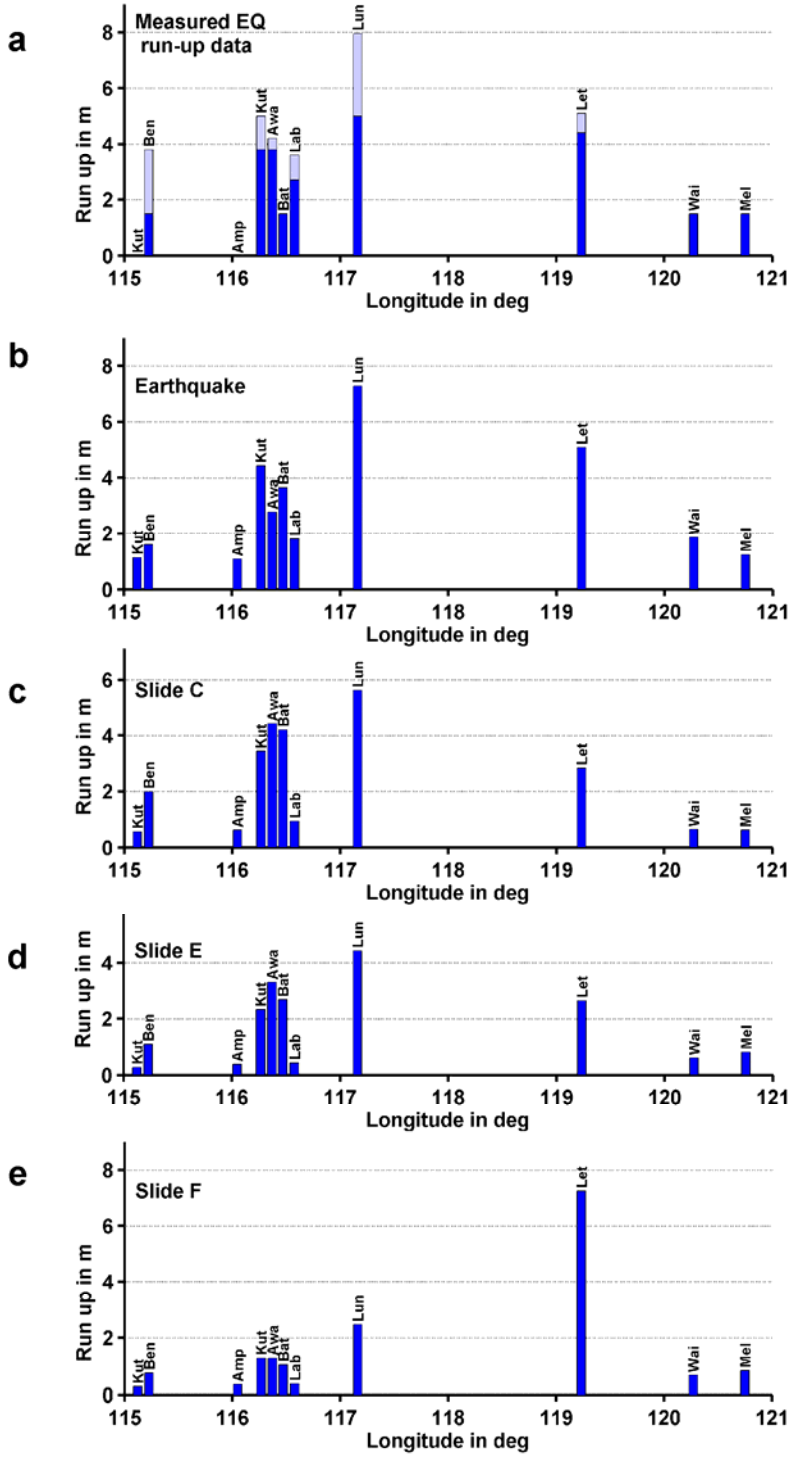

Figure 6 *Run-up distributions.* ***(a)*** *Measured run-up of the 1977 Sumba earthquake. If more than one value was measured at a location, light blue bars show the maximum run-up, while dark blue bars correspond to the minimum run-up.* ***(b)*** *Estimated run-up caused by the 1977 Sumba earthquake.* ***(c,d,e)*** *Modeled landslide-generated run-up heights for slides C, E and F, respectively. Measurement locations are mapped in Figure 5.*

empirical scaling relations of Wells and Coppersmith (1994). All other parameters are taken from the Global CMT Catalog: magnitude M_w 8.3, scalar moment $3.59 \cdot 10^{21}$ Nm, dip angle 67°, slip angle -98° and depth 23.3 km. In contrast to Kato and Tsuji (1995), we use the steeper of the two possible fault plane solutions which dips southward. In their paper, Kato and Tsuji (1995) assumed the Sumba event to be of the same type as the 1933 Great Sanriku earthquake and decided in favor of the shallow, northward dipping fault plane solution. However, a conjugate set of steeply northward and southward dipping normal faults dominate the morphology of the oceanic crust in the eastern Java trench (Müller et al. 2008; van der Werff 1995). The resemblance in strike and dip angle with the CMT fault mechanism of the 1977 Sumba earthquake clearly favors the southward dipping focal mechanism solution. Assuming a rigidity modulus of 30 GPa, we assess the co-seismic slip to be 9.5 m. Initial sea surface deformation is calculated according to Okada (1985), using the software AVI-NAMI v1.2 (Pelinovsky et al. 2006). We compute maximal subsidence of -3.3 m towards southeast and maximal uplift of 1.1 m in the opposite direction. Estimated run-up heights at surveyed locations are shown in Figure 6b. They exhibit only minor discrepancies to measured values (compare with Figure 6a).

Interestingly, modeled results for the second, perpendicular fault plane solution of the CMT catalog are quite similar. The initial maximal depression amounts to -3.6 m and the maximum elevation is 0.9, the distribution appears to be shifted slightly southward, but the overall shape is likewise. This explains why the tsunami model calculated by Kato and Tsuji (1995) exhibited similarly good correspondence with measured run-up values.

To test whether the presented landslides were triggered by the Sumba earthquake, we also calculate tsunami run-up heights for slides C, E, and F at the survey locations. As slide D induces only a negligible tsunami (maximum estimated run-up is 40 cm), it will not be discussed. Results are depicted in Figure 6c, d and e, respectively. The run-up distribution due to slide C exhibits a similar pattern as the earthquake. The same is true for slide E, but with somewhat smaller amplitudes. If one of these slides were triggered by the earthquake, the corresponding wave fields would superpose at each time step. This does not mean that the maximum run-up values have to be added at each location. They rather depend on the exact timing of the slide failure with respect to the earthquake's main shock. If the largest slide-induced wave arrives several minutes after the highest wave of the earthquake tsunami, it might not contribute to the run-up distribution. As the earthquake tsunami simulation corresponds well with the surveyed run-up values, we can only conclude, that no such superposition can be evidently observed at the given locations.

Slide F however, shows a different picture. In this case, the estimated run-up at Leterua exceeds the measured value by about 2 m. One could deduce that this slide was not induced by the 1977 earthquake. However, this conclusion would be based on one data point only and, regarding the intrinsic error range of the simulation, appears to be premature.

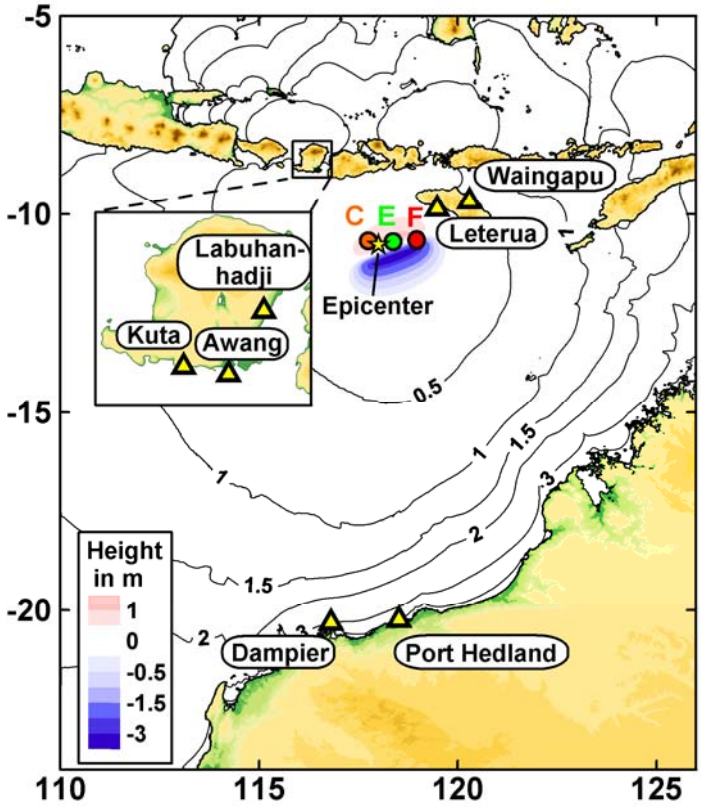

Figure 7 *Overview on stations with known tsunami arrival times. Shown are also slide locations C, E, F, the epicenter location and the initial earthquake tsunami pattern. Black lines designate earthquake tsunami arrival times in hours***.**

5.2 Comparison by arrival time

Another way of investigating whether one of the landslides contributed to the tsunami is the analysis of arrival times in Indonesia and Australia. The tsunami was recorded by gauges near Dampier and Port Hedland in Northwest Australia (Figure 7, Table 3). Two datasets of tide gauges are available at Dampier and further the record of a buoy near Legendre Island, 20 km north of Dampier. Wave arrival is strongly influenced by local bathymetry and we cannot resolve the extremely shallow island landscape off Dampier employing the GEBCO grid (resolution of 1 arc minute). Therefore, we use only the buoy data in the following discussion. Arrival times in Indonesia are reported by eyewitnesses on Lombok and Sumba. At Lombok, wave arrival was reported with reference to an interesting sound phenomenon: A noise similar to an explosion or aircraft sonic boom has been heard repeating three times. It was witnessed about 15 minutes after the earthquake trembling started (Kato and Tsuji 1995). These three noises have been reported independently in several locations on Lombok and Sumbawa. The first sign of tsunami arrival on Lombok, the receding of the water, were stated to happen few minutes after the sounds (ITIC 1977). Kato and Tsuji (1995) discussed the origin and timing of the noises, attributing the sounds to co-seismic rupture processes at the fault. According to their calculation of sound waves traveling in air, the noises reached Lombok 14 minutes after the seismic P-waves, which corresponds quite well to eye witness timing. We use this

Location	Measured data			Model simulations			
	Cited arrival time	Arrival time after EQ (6:09 UT)	Data source	EQ	Slide C	Slide E	Slide F
Leterua (Sumba)	~5 min after trembling	~5 min	ITIC (1977)	12 min	26 min	21 min	19 min
Awang (Lombok)	Almost immediately after noises	~16 min*	ITIC (1977)	31 min	30 min	35 min	40 min
Kuta (Lombok)	5 min after noises	~20 min*	ITIC (1977)	34 min	32 min	37 min	42 min
Labuhan-hadji (Lombok)	8 min after noises	~23 min*	ITIC (1977)	40 min	38 min	42 min	47 min
Waingapu (Sumba)	~1 h after trembling	~1 h	ITIC (1977)	62 min	63 min	62 min	59 min
Dampier (Australia)	8:59 UT	2:50 h	ITIC (1977)	3:02 h	3:04 h	3:02 h	3:05 h
Port Hedland (Australia)	~9:40 UT	~3:30 h	Gusman et al. (2009)	3:25 h	3:25 h	3:25 h	3:27 h

Table 3 *Tsunami arrival times. Compared are measured data and model simulations, ordered by arrival time. The locations are mapped in Figure 7.*

value to determine tsunami arrival times at Lombok (Table 3). It is important to note that eye witness accounts cannot be as exact as technical measurements. In Waingapu, for instance one witness reported wave arrival at roughly 1 hour after the trembling, while another stated it was only 10 min. (According to our results, it is very doubtful that the wave arrived at the far side of Sumba after 10 min.)

The computed tsunami arrival times in Table 3 designate the time span between the source event (earthquake or landslide) and the occurrence of a first large wave extremum at the survey location. The arrival time of the earthquake generated tsunami at Dampier and Port Hedland corresponds very well with local gauge records. Also for Leterua and Waingapu on Sumba, results of the earthquake model are quite consistent with eyewitness reports. However, the computed arrival of the earthquake tsunami at Awang, Kuta and Labuhanhadji on Lombok occurs roughly 15 minutes later as witnessed. The landslides presented in this study, can not be responsible for this discrepancy (Table 3). Even if one of them was triggered in the same instant as the main seismic shock, the resulting tsunami would not arrive 15 minutes before the earthquake tsunami. Two explanations for the discrepancy are possible. (1) The estimated travel time based on the survey data is erroneous, which could be due to somewhat incorrect eyewitness reports;

but most importantly the discrepancy appears only at locations where explosion sounds were used for the arrival estimation. It is important to recall that the source and travel mechanism of these noises is not proven. (2) A speculative, alternative explanation for the discrepancy would be a tsunami source in the fore-arc basin that was located roughly 170 km (corresponding to 15 min travel time at 3500 m water depth) closer to Lombok Island. Unfortunately, based on the available data, it is not possible to verify or falsify either of the explanations.

6 Conclusions

We identified six submarine landslides in new, high-resolution bathymetry data along the eastern Sunda trench. Three small events which involved between 1 and 4 km³ of sediments are located off Java, Lombok and Sumbawa. The remaining three landslides of significantly larger volumes (between 15 and 20 km³) are found at the margin toe off Sumba and Sumbawa.

Numerical modeling of landslide-generated tsunamis suggest that the largest events might have generated run-up heights of 7 m at Sumba, more than 5 m on Sumbawa and 3 m at Lombok Island. Maximum run-up on Bali and Java did not exceed 2 m.

As four slides are located directly above the assumed fault plane of the 1977 Sumba M_w=8.3 earthquake, we investigated if evidences for seismic landslide triggering could be revealed with the help of numerical modeling. Comparison of the measured run-up heights and arrival times to our tsunami simulations show that the earthquake tsunami model alone adequately explains most observations. This fact cannot, however, exclude co-seismic landslide triggering: the potential landslide tsunami might have propagated some time after the earthquake tsunami so that the waves did not measurably superpose at the survey points. Hence, based on the available data, we can neither support, nor decline the hypothesis of landslide triggering by the 1977 Sumba earthquake.

Acknowledgements

This is publication 25 of the GITEWS project (German Indonesian Tsunami Early Warning System). The project is carried out through a large group of scientists and engineers from GeoForschungsZentrum Potsdam (GFZ) and its partners from DLR, AWI, GKSS, IFM-GEOMAR, UNU, BGR, GTZ, as well as from Indonesian and other international partner institutions. Funding is provided by the German Federal Ministry for Education and Research (BMBF), grants 03TSU01 (GITEWS) and 03G0190 (SINDBAD).

Supplementary material

7 Study of run-up estimation

The run-up formula that we apply can be evaluated at any depth d that is bigger than the wave height itself (Ward and Asphaug 2003): $R = A^{4/5} \cdot d^{1/5}$, where A is the wave amplitude, measured at water depth d. To check the stability of run-up predictions in our models, we systematically vary the depth d between 250 m and 20 m while observing the resulting run-up heights. This parametric study is done near Sedjorong, southwest Sumbawa, as it is located in the center of our study area (see Figure 4). Other places, however, show very similar characteristics. The run-up formula is applied at six different positions off-shore (Figure 8a) for five tsunami models, generated by slides B to F (Figures 8b to 8f, respectively). In these figures, the input wave height A, which is the maximum wave height from the propagation simulation, is shown by the black portion of each bar. The whole bar represents estimated coastal run-up R. As indicated above the bars, gauges are sorted from left to right with decreasing depth d.

Off-shore wave heights A increase continuously by a factor of at least 2 during the shoaling process. Predicted run-up tends to increase as well, however, with distinctly smaller amplification factors. Generally, run-up estimates of the same event vary not more than 20 %. This means that the run-up formula can be applied at any depth between 250 m and 20 m without significantly affecting the final result.

8 Initial wave characteristics: Summary of Watts' and Grilli's approach

The generation part of our tsunami model consists of a couple of analytical and semi-empirical equations that have been proposed in publications of Watts, Grilli and coworkers. Here, we want to concisely summarize their approach and the formulas we applied in this publication. For the complete line of argumentation involved in this formulation, we refer to the original publications (Watts et al. 2003; Grilli and Watts 2005; Watts et al. 2005).

The approach is divided in two distinct parts. First, the slide event is described as a pure center of mass movement. The associated equations are derived analytically. Second, a numerical computation of many slides is conducted whereby all slides follow the analytical equations of the first part. This yields the dependency of characteristic tsunami parameters on the input slide variables in a semi-empirical way.

For the first part only one horizontal dimension (1HD) is considered. The submarine mass failure is idealized as an elliptic body, resulting in a landslide that can be described with relatively few parameters. The body's length, maximum thickness and initial submergence are denoted b, T and d, respectively (Figure 9). Failure occurs at a slope of inclination θ.

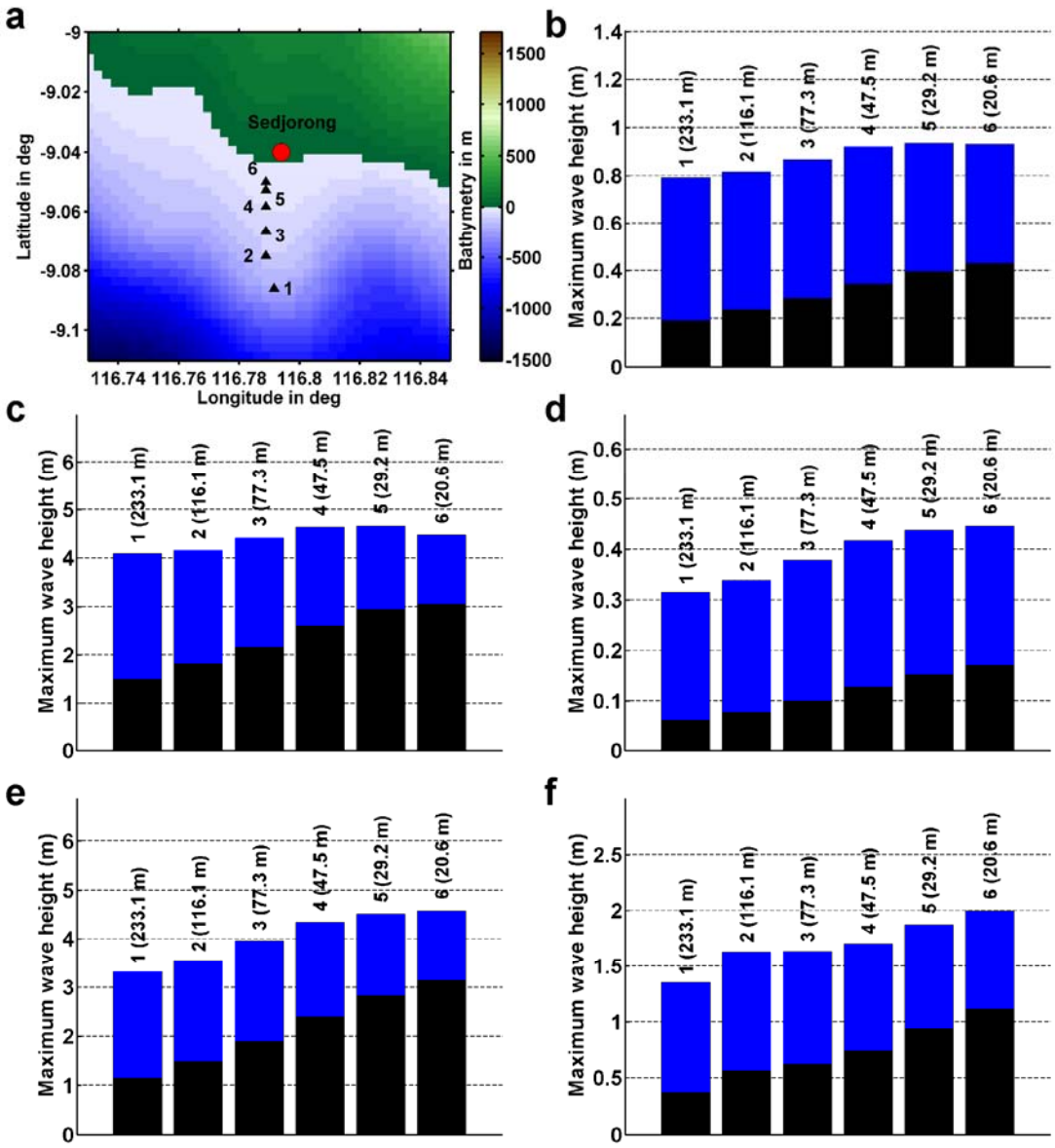

Figure 8 *Testing run-up predictions according to the relation of Ward and Asphaug (2003) for consequently decreasing depths of reference points.* ***(a)*** *Virtual gauge positions. The location of Sedjorong is mapped in Figure 4.* ***(b-f)*** *Black bars designate computed offshore wave heights (at reference points). Blue bars show extrapolated run-up values for each reference point. Labels are gauge numbers with respective depths. Subplot numbers b to f correspond to slide scenarios B to F, respectively.*

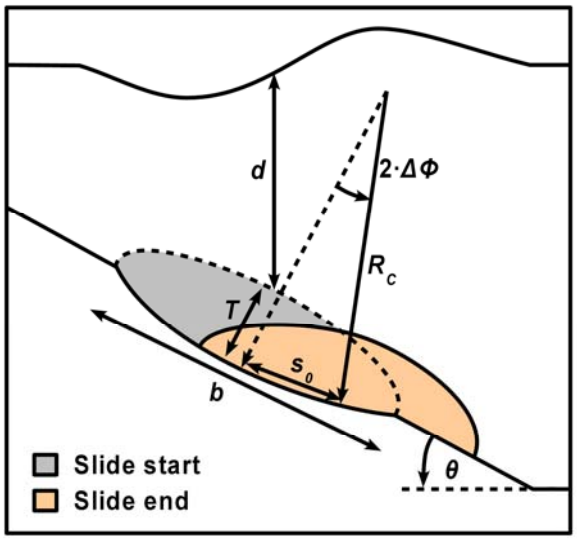

Figure 9 *Parameterization scheme after Watts et al. (2003). Displayed are submergence depth* d*, slide length* b*, travel distance* s_0*, slide height* T*, slope angle* θ*, slump radius of curvature* R_C *and angular displacement at moment of maximum velocity* ΔΦ.

The movement of the underwater slide is described by a sinusoidal center of mass trajectory *s(t)*:

$$s(t) = s_0\left[1 - \cos\left(\frac{t}{t_0}\right)\right]$$

This description is applicable for $t<\pi \cdot t_0$ where t_0 is the characteristic time of slump motion. Thus, a maximum velocity is produced in the middle of slump motion, while at slide start and end it equals zero. It is argued that almost all tsunami generation takes place during the first part of the movement, the acceleration phase. The angular displacement at the moment of maximum velocity is designated $\Delta\Phi$. It can be expressed in terms of the radius of curvature R_C and travel distance s_0:

$$\Delta\phi \cong \frac{2s_0}{R_C}$$

The above description uses a slump radius of curvature R_C that can be difficult to identify in bathymetric data. Thus, Watts et al. (2005) assume a parabolic failure surface which yields a simple analytical solution for the radius of curvature in terms of slide length *b* and thickness *T*:

$$R_C \cong \frac{b^2}{8T}$$

For the computation of initial acceleration a_0, maximum velocity u_{max} and the characteristic time of motion t_0 a specific slide density of 1.85 is assumed:

$$a_0 \cong 0.15 \cdot g \cdot \Delta\phi$$

$$u_{\max} \cong 0.27 \cdot \Delta\phi \sqrt{R_C \cdot g}$$

$$t_0 = \frac{u_{\max}}{a_0} \cong 1.84 \cdot \sqrt{\frac{R_C}{g}}$$

Thereby Coulomb friction coefficient is neglected, while added mass coefficient and drag coefficient are approximated by 1. The characteristic time of motion t_0 plays a special role as it designates the moment, when the initial tsunami shape is introduced as starting condition to the tsunami propagation model.

In the second part, the numerical tsunami generation models of Grilli and Watts (1999) and Grilli et al. (2002) are used that are based on the fully nonlinear potential flow equations solved with a Boundary Element Method. This method is applied to many landslides that move according to the center of mass description that we summarized above. As a result, the characteristic tsunami wavelength λ and the initial 1HD wave height η_{1HD} are expressed in terms of landslide parameters:

$$\lambda \equiv t_0 \sqrt{g \cdot d} \cong 1.84 \sqrt{R_C \cdot d}$$

$$\eta_{1HD} \cong 0.0654 \cdot T \cdot \Delta\phi^{1.39} (\sin\theta)^{0.25} \left(\frac{b}{d}\right)^{1.25} \left(\frac{R_C}{b}\right)^{0.37}$$

Up to now, only one horizontal dimension have been considered. Hence, η_{1HD} can be used for slides, where slide length b is much smaller than slide width w. In real cases, however, the effect of finite width can not be neglected and two horizontal dimensions (2HD) have to be taken into account. Based on mass conservation, Watts and Grilli (2005) suggest the following conversion from 1HD to 2HD initial wave height:

$$\eta_{2HD} = \eta_{1HD} \left(\frac{w}{w + \lambda}\right)$$

References

Bondevik S, F Løvholt, C Harbitz, J Mangerud, A Dawson, JI Svendsen (2005) The Storegga Slide tsunami - comparing field observations with numerical simulations. Mar Pet Geol. 22:195–208

Borrero JC, CE Synolakis, H Fritz (2006) Northern Sumatra field survey after the December 2004 Great Sumatra earthquake and Indian Ocean tsunami, Great Sumatra Earthquakes and Indian Ocean Tsunamis of December 26, 2004 and March 28, 2005. Earthq Spectra. 22

Chesley SR, SN Ward (2006) A Quantitative Assessment of the Human and Economic Hazard from Impact-generated Tsunami. Nat Hazards. 38:355–374

Eva C, M Cattaneo, F Merlanti (1988) Seismotectonics of the central segment of the Indonesian Arc. Tectonophys. 146:241-259

Fine IV, AB Rabinovich, BD Bornhold, RE Thomson, EA Kulikov (2005) The Grand Banks landslide-generated tsunami of November 18, 1929: preliminary analysis and numerical modeling. Mar Geol. 215:45-57

Fritz H, W Kongko, A Moore, B McAdoo, J Goff, C Harbitz, B Uslu, N Kaligeris, V Titov, CE Synolakis (2007) Extreme run-up from the 17 July 2006 Java tsunami. Geophys Res Abstr. 9, 10765

Geist EL, T Parsons (2006) Probabilistic Analysis of Tsunami Hazards. Nat Hazards. 37:277-314

Grilli, ST, P Watts (1999) Modeling of waves generated by a moving submerged body: Applications to underwater landslides. Eng Analysis with Boundary Elements. 23(8):645–656

Grilli, ST., S Vogelmann, P Watts (2002) Development of a 3-D numerical wave tank for modeling tsunami generation by underwater landslides. Eng Analysis with Boundary Elements. 26(4):301–313

Grilli ST, P Watts (2005) Tsunami generation by submarine mass failure Part I: Modeling, Experimental Validation, and Sensitivity Analyses. J Waterway Port Coastal and Ocean Eng. 131(6):283-297

Gusman AR, Y Tanioka, H Matsumoto, SI Iwasaki (2009) Analysis of the Tsunami Generated by the Great 1977 Sumba Earthquake that Occurred in Indonesia. Bull Seism Soc Am. 99(4): 2169–2179, doi: 10.1785/0120080324

Hall R (1997) Cenozoic plate tectonic reconstructions of SE Asia. Geological Society Special Publications 126:11-23

Hamzah L, NT Puspito, F Imamura (2000) Tsunami Catalog and Zones in Indonesia. J Nat Disaster Sci. 22(1):25-43

Harbitz CB (1992) Model simulations of tsunamis generated by the Storegga slides. Mar Geol. 105:1-21

Hébert H, A Piatanesi, P Heinrich, F Schindelé (2002) Numerical modeling of the September 13, 1999 landslide and tsunami on Fatu Hiva Island (French Polynesia). Geophys Res Lett. 29(10):1484

Heine C, RD Müller, C Gaina (2004), Reconstructing the lost Thethys Ocean basin: Convergence history of the SE Asian margin and marine gateways. In: P Clift, P Wang, W Kuhnt and D Hayes (eds) Geophysical Monograph Series Vol 149: Continent-Ocean interactions within East Asian marginal seas, AGU, Washington DC, pp 37-54

IOC, IHO and BODC (2003) Centenary Edition of the GEBCO Digital Atlas, British Oceanographic Data Centre, Liverpool

ITDB/WLD (2007) Integrated Tsunami Database for the World Ocean, Version 6.51 of February 20, 2007. CD-ROM, Tsunami Laboratory, ICMMG SD RAS, Novosibirsk, Russia

ITIC (International Tsunami Information Center), Tsunami reports No. 1977-12

Imamura F, N Shuto, C Goto, Y Ogawa, (1997) IUGG/IOC Time Project IOC Manuals and Guides No.35, (UNESCO)

Kato K, Y Tsuji (1995) Tsunami of the Sumba earthquake of August 19, 1977. J Nat Disaster Sci. 17(2):87-100

Kopp H, N Kukowski (2003) Backstop geometry and accretionary mechanics of the Sunda margin. Tectonics 22(6):1072.

Kopp H, ER Flueh, CJ Petersen, W Weinrebe, A Wittwer, Meramex Scientists (2006) The Java margin revisited: Evidence for subduction erosion off Java. Earth Planet Sci Lett. 242:130–142

Kukowski N, A Hampel, S Hoth, J Bialas (2008) Morphotectonic and morphometric analysis of the Nazca plate and the adjacent offshore Peruvian continental slope - Implications for submarine landscape evolution. Mar Geol. 254:107-120

Lavigne F, C Gomez, M Giffo, P Wassmer, C Hoebreck, D Mardiatno, J Prioyono, R Paris (2007) Field observations of the 17 July 2006 Tsunami in Java. Nat Hazards Earth Syst Sci. 7:177–183

Lynett P, PLF Liu (2002) A numerical study of submarine-landslide-generated waves and run-up. Proc R Soc A. 458:2885

Lynett PJ, JC Borerro, PLF Liu, CE Synolakis (2003) Field Survey and Numerical Simulations: A Review of the 1998 Papua New Guinea Tsunami. Pure Appl Geophys. 160:2119–2146

Lynnes CS, T Lay (1988) Source Process of the Great 1977 Sumba Earthquake. J Geophys Res. 93(Bll):13,407-13,420

Masson DG, LM Parson, J Milsom, G Nichols, N Sikumbang, B Dwiyanto, H Kallagher (1990) Subduction of seamounts at the Java Trench: a view with long-range sidescan sonar. Tectonophys. 185:51– 65

Masson DG, CB Harbitz, RB Wynn, G Pedersen, F Løvholt (2006) Submarine landslides: processes, triggers and hazard prediction. Phil. Trans R Soc A. 364:2009-2039

Matsumoto T (2007) An underwater landslide or slump on an active submarine fault - A possible source of a devastating tsunami? Eos Trans AGU. 88(52), Fall Meet. Suppl., Abstract S53A-1018

McAdoo B, G Simpson (2005) Morphometric dating of submarine landslide scarps. Geophys Res Abstr. 7, Abstract 00629

Moran K, D Tappin (2006) SEATOS 2005 Cruise Report: Sumatra Earthquake and Tsunami Off shore Survey (SEATOS). 92 pp. (Online) available at http://ocean.oce.uri.edu/seatos.

Müller C, H Kopp, YS Djajadihardja, U Barckhausen, Ehrhardt A, Engels M, Flueh ER, Gaedicke C, Keppler H, Lutz R, Lüschen E, Neben S, Seeber L, Dzulkarnaen DPS (2008) From subduction to collision; The Sunda-Banda Arc transition. Eos, Transactions, American Geophysical Union 89:49-50

Okada Y (1985) Surface deformation due to shear and tensile faults in a half-space. Bull Seism Soc Am. 75(4):1135-1154

Pelinovsky E, A Kurkin, A Zaytsev, A Yalciner, F Imamura (2006) AVI-NAMI Version 1.2

Rynn J (2002) A preliminary assessment of tsunami hazard and risk in the Indonesian region. Sci Tsunami Hazard. 20(4):193

Satake K (1988) Effects of Bathymetry on Tsunami Propagation: Application of Ray Tracing to Tsunamis. Pure Appl Geophys. 126(1):27-36

Schlueter HU, C Gaedicke, HA Roeser, B Schreckenberger, H Meyer, C Reichert, Y Djajadihardja, A Prexl (2002) Tectonic features of the southern Sumatra-western Java forearc of Indonesia. Tectonics. 21(5):15

Simons WJF, A Socquet, C Vigny, BAC Ambrosius, S Haji Abu, C Promthong, C Subarya, DA Sarsito, S Matheussen, P Morgan, W Spakman (2007) A decade of GPS in Southeast Asia: Resolving Sundaland motion and boundaries. J Geophys Res. 112

Spence W (1986) The 1977 Sumba Earthquake Series: Evidence for Slab Pull Force Acting at a Subduction Zone. J Geophys Res. 91:7225-7239.

Sweet S, EA Silver (2003) Tectonics and Slumping in the Source Region of the 1998 Papua New Guinea Tsunami from Seismic Reflection Images. Pure Appl Geophys. 160:1945–1968

Synolakis CE, JP Bardet, JC Borrero, HL Davies, EA Okal, EA Silver, S Sweet, DR Tappin (2002) The slump origin of the 1998 Papua New Guinea Tsunami. Proc R Soc Lond A. 458:763–789

Tappin DR, T Matsumoto, P Watts, K Satake, GM McMurtry, M Matsuyama, Y Lafoy, Y Tsuji (1999) Sediment slump likely caused 1998 Papua New Guinea tsunami. Eos Trans AGU. 80(30):329

Tappin DR, LC McNeil, T Henstock, D Mosher (2007) Mass wasting processes - offshore Sumatra. In: V Lykousis, D Sakellariou, J Locat (eds) Advances in Natural and Technological Hazards Research Vol 27: Submarine Mass Movements and Their Consequences, Springer, Dordrecht, pp 327-336

Titov VV, CE Synolakis (1997) Extreme inundation flows during the Hokkaido-Nansei-Oki tsunami Geophys Res Lett. 24(11):1315-1318

Tsuji Y, F Imamura, H Matsutomi, CE Synolakis (1995a) Field Survey of the East Java Earthquake and Tsunami of June 3, 1994. Pure Appl Geophys. 144(3/4):839

Tsuji Y, H Matsutomi, F Imamura, M Takeo (1995b) Damage to Coastal Villages due to the 1992 Flores Island Earthquake Tsunami. Pure Appl Geophys. 144(3/4):481

Tsuji Y, Y Namegaya, H Matsumoto, SI Iwasaki, W Kanbua, M Sriwichai, V Meesuk (2006) The 2004 Indian tsunami in Thailand: Surveyed runup heights and tide gauge records. Earth Planet Space. 58:223-232

UHSLC (University of Hawai, Sea Level Center) 2008 http://ilikai.soest.hawaii.edu/

van der Werff W (1995) Structure and morphotectonics of the accretionary prism along the Eastern Sunda-Western Banda Arc. J Southeast Asian Earth Sci. 11:309-322.

Ward SN, E Asphaug (2003) Asteroid impact tsunami of 16 March, 2880. Geophys J Int. 153:F6–F10

Watts P, ST Grilli, JT Kirby, GJ Fryer, DR Tappin (2003) Landslide tsunami case studies using a Boussinesq model and a fully nonlinear tsunami generation model. Nat Hazards Earth Sys Sci. 3:391-402

Watts P, ST Grilli, DR Tappin, GJ Fryer (2005) Tsunami Generation by Submarine Mass Failure. II: Predictive Equations and Case Studies. J Wtrwy Port Coast Oc Eng. 131:283

Wells DL, KJ Coppersmith (1994) New Empirical Relationships among Magnitude, Rupture Length, Rupture Width, Rupture Area, and Surface Displacement. Bull Seism Soc Am. 84(4):974-1002